# DESIGN OF AN X-RAY IMAGING SYSTEM TO ANALYSE CORIUM-WATER INTERACTION

V. Moulin[1], J. Tabary[1], M. Antonakios[1] and P. Fouquart[2]
[1] CEA-DRT/DTBS ; Grenoble ; France; [2] CEA-DEN/DTP ; Cadarache ; France

**Abstract:** The Krotos experience requires fast imaging (10 to 100 images/sec) of a dynamic process involving highly attenuating corium (density 8) and detection of low density variations (distinction between water and steam), with millimetric spatial resolution. In response to this difficult problem, various solutions were devised and simulated. We will show that the only feasible option is to use a very high energy (8 MeV) and very powerful source (0.3 Gy/s), associated with a scintillator screen optically linked to a high sensitivity CCD camera. This solution has been validated in the experimental phase to ensure its performance: results confirm the possibility of monitoring with 10 images/sec with a single X flash per image.

**Introduction:** The study of "**serious accidents**" involves imagining the case of a nuclear reactor core fusion: resulting from a cooling fault, all structures (mainly zircaloy) and nuclear fuel (in uranium oxide form, to which fission products are added) melt to form a liquid called "**corium**". Depending on the scenario envisaged, this may break through the main tank and flow into the building hall. Starting up the spray system (normally used in the event of incidents to cool the tank), the hall floor can be flooded with several tens of cm of water.
In this context, the corium-water interaction requires careful examination. The heat energy provided by the corium is such that a risk of **steam explosion** is potentially possible. Studies therefore attempt to find out more about the corium–water interaction, to determine the conditions favourable to steam explosion and assess the energy dissipated by such an explosion. In particular, the development of a simulation tool must compare its results with experimental data.
To study the corium–water interaction, various experimental systems have been produced throughout the world. Among them, the experimental system **Krotos** [1, 2] enables liquid corium, heated to 2800°C to be poured in a test section (internal diameter 200 mm) filled with water. The aim is to determine the parameters of the pre-mix obtained: number and size of corium fragments, location of the so-called “coherent” (unfragmented) jet, location and size of the vapour films formed around the corium. These phenomena occur very quickly: the jet of corium propagates in the water at a speed of 3 m/sec, and the experiment only lasts a few seconds. The objective is to monitor these experiments with millimetric spatial resolution, at a rate of 10 to 100 images per second.
Visible observations are rapidly unusable because of the water vaporisation caused by the melted metal. Use of an X-ray imaging system was therefore envisaged.
After weighing up the problem, we will present the simulation results for a number of configurations, then the experiment results obtained on a high energy system. We will then explain the differences observed between the simulations and experiments and the apparent contradiction between our results and those obtained by other systems.

**Method:** An imaging system is a compromise between three parameters: integration duration, spatial resolution and measurement accuracy (or density resolution). Improving one of these parameters always leads to deterioration of one or both of the others.
In the Krotos experiment, the challenge is a tricky one, as the system must be very fast, with quite accurate precision to distinguish a vapour film in the water, while penetrating the corium, and all this with millimetric spatial resolution that remains restrictive in the light of the other requirements. In other words, the compromise between the three above-mentioned parameters will be difficult to determine.
First, we devised not one but two imaging chains, operating simultaneously. Each chain is turned 90° from the other. One, called "low energy" (**LE**; X generator of 100 to 400 kV) aims to view

the vapour film; the other, called "high energy" (**HE**; linear electron accelerator, maximum energy greater than 1 MeV) is used to observe fragments and the coherent jet.
A dual system of this kind has been used by Wisconsin-Madison university, to monitor an analog experiment [3]. We have these results that actually show the ability of the LE chain to view a vapour film around the corium jet. The results of the HE chain are less convincing however, with only slight contrast, which seriously limits location of the coherent jet.
In view of the speed restrictions and current technologies, a system using a scintillator screen, optically linked to a camera seemed to be the only viable solution. This solution has already been tested in HE dynamic inspection systems [4, 5]. Another technology, using CdZnTe strip detectors [6, 7] was also envisaged. However, the dynamic aspect of the Krotos experiment prevents radiography by translation scanning and this detector can only give a series of profiles.

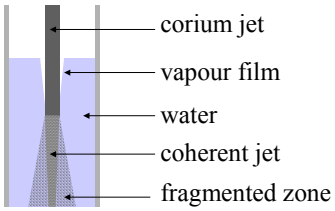

Figure 1: diagram of experiment principle

Hereafter, we will concentrate on detecting the vapour film, particularly because it enables comparison of results of the LE and HE systems. Only one example of the coherent jet location shall be given.
The traditional Berr-Lambert law [8] is used to express the attenuation of the X-ray through the Krotos system. To simplify expression of the relationships, we will use a monochromatic radiation, corresponding to the average energy $E_{ave}$ of the emission spectrum. This gives:

$$I = I_0 . e^{-(\mu l)_{structures}} e^{-\mu_{water} l_{water}} e^{-\mu_{corium} l_{corium}} e^{-\mu_{vapour} l_{vapour}} \quad (1)$$

The term $(\mu l)_{structures}$ represents attenuation of the experiment system structures (enclosure windows, test section), constant attenuation over time. It should indeed be pointed out that the test section is itself placed within a cylindrical enclosure able to resist the overpressure generated by a steam explosion. It is therefore only possible to view the corium flow through this enclosure, equipped with observation windows (cumulated thickness approximately 30 mm of aluminium).
Furthermore, because of the very low density of the vapour, we will henceforth consider:

$$e^{-\mu_{vapour} l_{vapour}} \approx 1 \quad (2)$$

Over a given trajectory, the thicknesses $l_{water}$, $l_{corium}$, and $l_{vapour}$ evolve as the experiment progresses, but the length of the test section crossed remains constant over time. By noting this length $l_{tot}$, we can check the following equation at any moment:

$$l_{water} + l_{corium} + l_{vapour} = l_{tot} \quad (3)$$

Before corium flow, we can make the following initial measurement:

$$I_{ini} = I_0 . e^{-(\mu l)_{structures}} e^{-\mu_{water} l_{tot}} \quad (4)$$

If we initially consider a source–pixel detector trajectory that is free of corium (the vapour film can only be viewed on this type of trajectory, as the corium is too attenuating). Relationships (1) to (4) enables the following to be established:

$$l_{vapour} = \frac{-1}{\mu_{water}} \cdot \ln \frac{I_{ini}}{I} \quad (5)$$

We can therefore see that the imaging system is potentially able to estimate the thickness of steam present on the given trajectory in the absence of corium. The noise associated with this measurement is given by:

$$\sigma_{lvapour} \approx \frac{1}{\mu_{water}} \cdot \frac{\sigma_I}{I} \quad (6)$$

We assume that the initial image is acquired with an excellent statistic to make its noise negligible compared with that of a unit image acquired during the experiment.
Reading this relationships shows that a LE solution seems, *a priori,* more suitable, because at low energy, $\mu_{water}$ attenuation is higher, which tends to reduce noise on the estimation of the vapour thickness.
Hereafter, we have determined and compared the performances of the various imaging chains envisaged, by quantifying the noise $\sigma_{lvapour}$ on the vapour thickness.

**Simulation results:** In the first phase, we used simulation to determine the respective performances of each chain: LE and HE. To do so, we used the CEA-LETI's simulation software Sindbad [9]. The first, purely analytical, level of this software is a calculation code based on:

- description of the radiation source (source X using Birch & Marchal's model or Gamma source);
- radiation-material interaction (in the object being X-rayed), of the direct flow exponential attenuation type (Storm and Israël's attenuation coefficients, and material mixing);
- energy deposit in the detector then a conversion to a signal, depending on the type of detector (with addition of noise and resolution effects depending on the simulated detector).

Using Sindbad, we will determine the energy deposited in the scintillator $E_{abs}$ and the associated noise $\sigma_{abs}$. Sindbad also provides $E_{ave}$, the average energy of the radiation absorbed in the scintillator. We can then calculate the accuracy on the vapour thickness (see (6)):

$$\sigma_{lvapour} \approx \frac{1}{\mu_{water}(E_{ave})} \cdot \frac{\sigma_{abs}}{E_{abs}} \qquad (7)$$

It should be noted that at this level, we are only considering the photonic noise and not yet the noise due to optical coupling and the measurement electronics (CCD camera).
This enables us to deduce the vapour film detection limit for different measurement chains. Table 1 presents the results obtained for two LE solutions and two HE solutions:

- 90 kV 200 mA generator with short exposure period: this type of generator is that used for the experiments carried out in Winsconsin university, Madison
- 400 kV 1.25 mA generator (traditional system)
- low power linear accelerator (0.02 Gy/s)
- Minilinatron or Varian 2000 type linear accelerator (0.3 Gy/s)

The scintillator used is suited to the energy field used, i.e.:

- LE: 1 mm gadox (35 to 40% stopping power at 400 kV)
- HE: 1.5 mm $Gd_2O_2S$ + 1 mm reinforcing tantalum (approx. 11% stopping power at 6 MeV)

These results show the clear superiority of a HE system with high dose output (0.3 Gy/s): the signal to photonic noise ratio is very favourable and enables significant compensation of the fact that the attenuation coefficient $\mu_{water}$ is lower for this energy field (see relationship (6)).

| | 90 kV 200 mA | 400 kV 2.25 mA | Linear accelerator | |
|---|---|---|---|---|
| | | | 0.02 Gy/s | 0.3 Gy/s |
| $\mu_{water}$ ($E_{ave}$) ($cm^{-1}$) | 0.203 | 0.159 | $4.99.10^{-2}$ | $4.52.10^{-2}$ |
| $E_{abs}$ (keV) | $1.36.10^{5}$ | $1.50.10^{5}$ | $1.30.10^{7}$ | $8.92.10^{7}$ |
| $\sigma_{abs}$ (keV) | $9.95.10^{3}$ | $4.95.10^{3}$ | $1.26.10^{5}$ | $4.02.10^{5}$ |
| $\sigma_{lvapour}$ (mm) | 1.1 | 2.1 | 1.9 | 0.10 |

Table 1: accuracy of the vapour thickness for different imaging chains
photonic noise only, pixel 1 mm², integration duration10 ms

Using the double HE and LE imaging system, we also studied the influence of the scattered radiation from a source on the detector of the other imaging chain. We were able to simulate this aspect with the MC (Monte-Carlo) function of the Sindbad simulation software [10, 11]. The main results of this study are presented in table 2. They show that the direct signal of the HE chain, even attenuated by 30 mm of corium, still remains superior to the scattered components from LE and HE. On the other hand, the direct LE signal (without corium) and the scattered radiation from HE are of the same order of magnitude. Although the component added by the scattered radiation, low frequency, can easily be subtracted from the image, it adds photonic noise that is impossible to eliminate.

| | Direct signal | Intrinsic scattered signal | Scattered signal from the other chain |
|---|---|---|---|
| LE detector (presence of water only) | LE → LE | LE → LE | HE → LE |
| | $3.44.10^7$ | $6.43.10^6$ | $5.24.10^7$ |
| HE detector (behind 30mm of corium) | HE → HE | HE → HE | LE → HE |
| | $4.98.10^9$ | $7.08.10^8$ | $3.65.10^7$ |

Table 2: mutual influences of scattered radiation
(levels expressed in $keV.mm^{-2}.s^{-1}$)

To ensure realistic results, we have to integrate the measurement chain noise in our simulation. We have empirical knowledge of $\sigma_{elec}$, the noise induced by the optical and electronic chain for a level of luminosity representative of a HE full flow level. We assume constant noise regardless of the level of luminosity.
To provide reliable results for experimentalists, we concentrated on the realistic case illustrated in figure 2 of a vapour film created around a corium jet of 50mm diameter: for this geometry, we establish the relationship between $l_{vapour}$, the thickness crossed by the X-ray at the centre of the film and the thickness $th_{vapour}$ of this film. This gives:

$$th_{vapour} = \frac{\sqrt{\Phi_{corium}^2 + 3.l_{vapour}^2} - \Phi_{corium}}{3} \qquad (8)$$

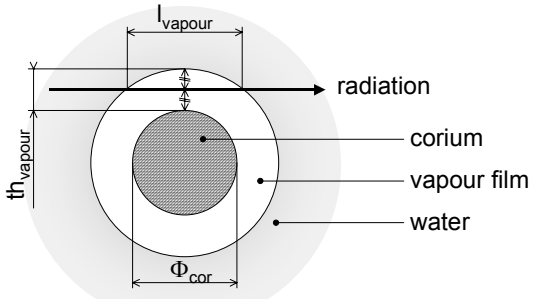


Figure 2: geometry of the vapour film around the coherent corium jet

Taking $l_{vapour} = 3\ \sigma_{lvapour}$, we can calculate the thickness of the detectable vapour film.
The results thus obtained are presented in table 3. They show the inability of the LE chains to provide images of the experiment at a high rate. A high energy solution using a low power accelerator is also unsuitable. Only use of a HE radiation source with a high dose output gives a totally acceptable result. Figure 3 shows an image simulated by Sindbad 3D corresponding to these conditions. The vapour film appears very clearly.

| | 90 kV 200 mA | 400 kV 2.25 mA | Linear accelerator | |
|---|---|---|---|---|
| | | | 0.02 Gy/s | 0.3 Gy/s |
| $\mu_{water}(E_{ave})$ ($cm^{-1}$) | 0.203 | 0.159 | $4.99.10^{-2}$ | $4.41.10^{-2}$ |
| Signal/Noise | $6.94.10^{-2}$ | $7.63.10^{-2}$ | 6.63 | 45.5 |
| $\sigma_{lvapour}$ (mm) | 710 | 820 | 30 | 4.9 |
| $th_{vapour}$ (mm) | 1200 | 1400 | 38 | 2.0 |

Table 3: accuracy of the vapour thickness and detectability limit of photonic and electronic noise, pixel 1 mm², integration duration 10 ms

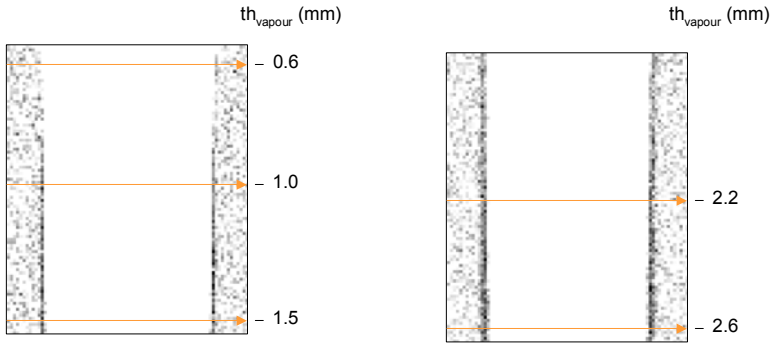


Figure 3: image simulated by Sindbad: source 6 MeV 0.3 Gy/s, 10 ms integration

**Experimental validation:** A second experimental phase concerned the HE system only. A so-called "static" mock-up was made: a cone of corium in water, all within a cast nylon test section. However, substitution materials had to be used:

- The corium (density 8) was replaced with an inert material, stainless steel (density 7.8);
- To obtain a vapour film between the water and the stainless steel, the water was replaced by a solid material of equal density: polyethylene (density 0.96).

On the images obtained, the emission profile and conicite effect of the mock-up increase the noise estimation unfavourably. To overcome these unwanted phenomena, we considered

$$S = \ln \frac{I_{ave}}{I} \tag{9}$$

Where I represents a unitary acquisition and $I_{ave}$ the average of more than 100 unitary images. This gives

$$\sigma_S \approx \frac{\sigma_I}{I} \tag{10}$$

taking $\sigma_I >> \sigma_{I_{ave}}$ in view of the high oversampling of $I_{ave}$. This then gives:

$$\sigma_{lvapour} \approx \frac{1}{\mu_{water}} \cdot \sigma_S \tag{11}$$

Different configurations were tested (geometry, camera pixel grouping, integration duration, shot frequency). Let's concentrate on the case most able to perform Krotos monitoring. The acquisition conditions are:

- source – detector distance: 1250 mm
- integration duration: 17 ms
- scintillator pixel surface area: 0.67 × 0.67 mm²
- accelerator frequency: 58 Hz, i.e. 1 shot / image

Compared to the case simulated in the first phase, the most important differences are pixel size ($1 \times 1$ mm² for the simulations), but above all, accelerator frequency, brought from 300 Hz to 58 Hz to ensure a 1 X flash / image mode. The dose output is therefore brought to 0.06 Gy/s.
In spite of these stricter conditions, the results are better than those predicted by simulation, as we obtained a S/N ratio of 110 (instead of 46 in table 3), which gives an accuracy on the $\sigma_{lvapour}$ vapour measurement of around 2 mm. This accuracy could potentially enable identification of a vapour film of a thickness $th_{vapour}$ (calculated according to (8)) of 0.4 mm !
The performance of these results must, however, be put into perspective, as shown by the image obtained on the mock-up, presented in figure 4. The vapour film detectability limit corresponds to a thickness of 1-2mm, not 0.4 as suggested by the noise analysis. The limiting factor is therefore the system's spatial resolution. Indeed, MTF (Modulation Transfer Function) measurements show a resolution limit at 0.4 pl/mm. This MTF is *a priori* independent of the acquisition conditions, in particular of the pixel grouping mode. The limit seems to come from criteria related to X-ray production and interaction phenomena, particularly the energy spread of a photon in the scintillator.

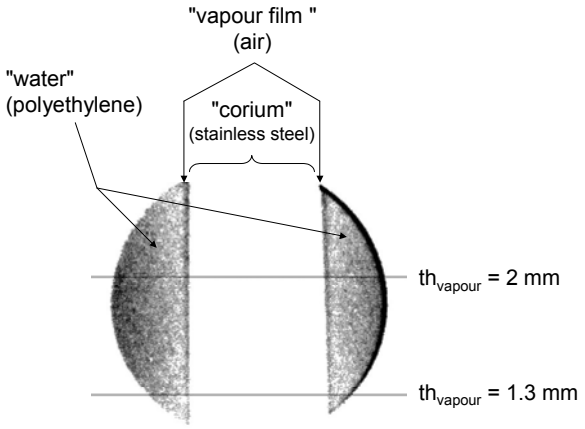


Figure 4: experimental image: vapour film around a corium jet (simulated by stainless steel); the altitudes marked on the image indicate film thickness $th_{vapour}$;
integration 17 ms; source 8 MeV, 0.06 Gy/s

**Discussion:** The simulation results, confirmed by experiments showing that a high dose output HE system (0.3 Gy/s) is totally able to detect a vapour film; furthermore, this is the only feasible solution.
These results can be explained simply: the signal emitted by the LE solutions is clearly less energetic that the one of the HE solutions. Indeed, table 1 shows a factor 100 at least on the absorbed energy. The photonic signal to noise ratio is unfavourable in LE, but above all, the luminosity induced in the scintillator is much lower. It is actually insufficient to be usable by a high sensitivity CCD camera over a short integration duration (10 ms). Only the level of luminosity generated by a very powerful energy system can be exploited. It must be remembered that these results take into account the relatively high attenuation induced by the Krotos experiment (windows, test section, water).

Our results contradict the images obtained in LE at Winsconsin university, Madison, on which the vapour film can be distinguished. However, this experiment differed from the Krotos case in that there was a smaller test section diameter and no outer enclosure. We simulated these conditions (geometry + 90 kV 200 mA generator) according to the information we had available. We obtained an accuracy $\sigma_{lvapour} = 18.5$mm. However, on the images we have, the vapour film is visible from thicknesses of around 3-6 mm (see figure 5) for a jet diameter (20 mm); this corresponds to respective vapour lengths of 12 mm to 18 mm. In view of the uncertainties due to certain incomplete data, we consider these results to be totally consistent.

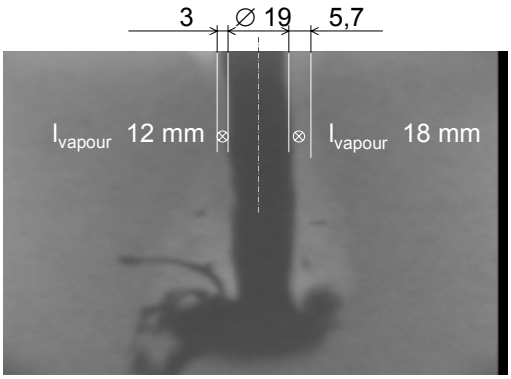

Figure 5: images obtained by Winsconsin university, Madison

As part of our study, the fact that the experiment results were better than the simulation can be explained by the modification of the acquisition geometry in relation to usual conditions. Monitoring the Krotos experiment requires a relatively small imaging field compared to previous applications. This enabled reduction of the source–scintillator distance as well as of the scintillator-camera distance, resulting in a light signal clearly superior to that considered in the simulation phase. However, we saw that the main limitation related to rapid acquisition is that it requires high luminosity behind the scintillator. Increased luminosity thus enabled a very rapid increase in image quality, much faster than the simple fact of having a better statistic concerning X photons.

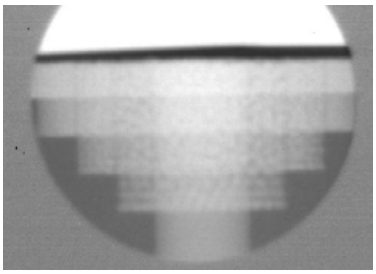
Figure 6: image of a steel bar (∅ 30 mm) sunk in steel balls
integration 9.7 ms; source 8 MeV, 0.1 Gy/s

At present, the system is limited by its spatial resolution. Tests carried out with more accurate scintillators tend to show that improvement is possible.. However, increasing scintillator accuracy implies reducing the stopping power, therefore deteriorating the signal to noise ratio: a compromise will therefore have to be found by integrating the definitive properties of the Krotos experiment and its enclosure.
It should also be noted that the HE system is totally able to locate the coherent part of the corium jet, as shown in figure 6: a steel bar, diameter 30mm, sunk in balls (representing the corium fragments) remains visible. The balls represent fragments of several diameters (54-126 mm for the upper ring).

**Conclusions:** The tests carried out enable affirmation that experiment monitoring at 58 images/sec will be possible with a high energy imaging system based on use of a powerful accelerator (0.3 Gy/s in nominal conditions). Furthermore, the images may be taken with a single accelerator flash, which gives a series of frozen images of the experiment.
This imaging system also enables the most dense corium zones to be crossed to locate the coherent part of the jet.
The set of experimental measurements, of which only one example is presented here, provided us with the data necessary to adjust our simulation model to the Krotos experiment monitoring problem. In parallel to our study, experiment definition is also evolving (modification of the

enclosure, test section). Ultimately, we will be able to integrate all these elements to define, and optimise by simulation, the imaging system best suited to the Krotos monitoring.
More generally, such an imaging system will be able to perform non-destructive radioscopic monitoring of several experimental or industrial processes, involving relatively attenuating materials.

**References:**


[1] D. Hohmann, D. Magallon, H. Schins, A. Yerkess, FCI Experiments in the aluminium oxide/water system, Nucl. Eng. Des. **155** (1995), 391-404.

[2] I. Huhtiniemi, D. Magallon, Insight Into Steam Explosions with Corium Melts in KROTOS, Nucl. Eng. Des. **204** (2001) 391-400.

[3] Eric P. Loewen, R. Bonazza, P. Chaopricha, M. Corradini, K. Cummings, C. Selig, G. Thomas, Dual-energy X-ray imaging to measure phase volume fractions in a transient multiphase flow, University of Wisconsin Madison, June 1999.

[4] P. Rizo, M. Antonakios, P. Lamarque, Tangential radiography detectability by tomosynthesis techniques, QNDE 1994, Snowmass Co., USA, pp361-368, 1994.

[5] M. Antonakios, P. Rizo, P. Lamarque, Real time tomosynthesis system applied to solid rocket motor examination, ECNDT, Copendhague (DK), may 26-29, 1998.

[6] F. Glasser, V Gerbe, P. Ouvrier-Buffet, M. Accensi, J.L. Girard, M. Renaud, J.L. Gersten-Mayer, CdZnTe high-energy radiography detector, Nuclear Instruments and Methods in Physics Research A458 (2001) 544-550.

[7] F. Glasser, P. Villard, J.P. Rostaing, M. Accensi, N. Baffert, J.L. Girard, Large dynamic range 64 channel ASIC for CZT or CdTe detectors, 4th International Workshop on radiation Imaging Detectors, Amsterdam, September 2002.

[8] E. Storm, H. Israel, Photon cross sections from 1 keV to 100 MeV for elements Z=1 to 100, Academic Press Inc, 1970.

[9] R. Guillemaud, J. Tabary, P. Hugonnard, F. Mathy, A. Koenig, A. Glière, Sindbad: a multi-purpose and scalable X-ray simulation tool for NDE and medical imaging, PSIP 2003, Grenoble, France, 2003

[10] J. Tabary, A. Glière, Coupling photon Monte Carlo simulation and CAD software. Application to X-ray non destructive evaluation, in *Proc. Monte Carlo 2000*, PP 461-466, Lisbon, Portugal, Oct. 23-26, 2000

[11] J. Tabary, A. Glière, R. Guillemaud, P. Hugonnard, F. Mathy, Combination of high resolution analytically computed uncollided flux images with low resolution Monte Carlo computed scattered flux images, *IEEE Transactions on Nuclear Science*, Vol. 51, No. 1, pp 212-217, Feb. 2004